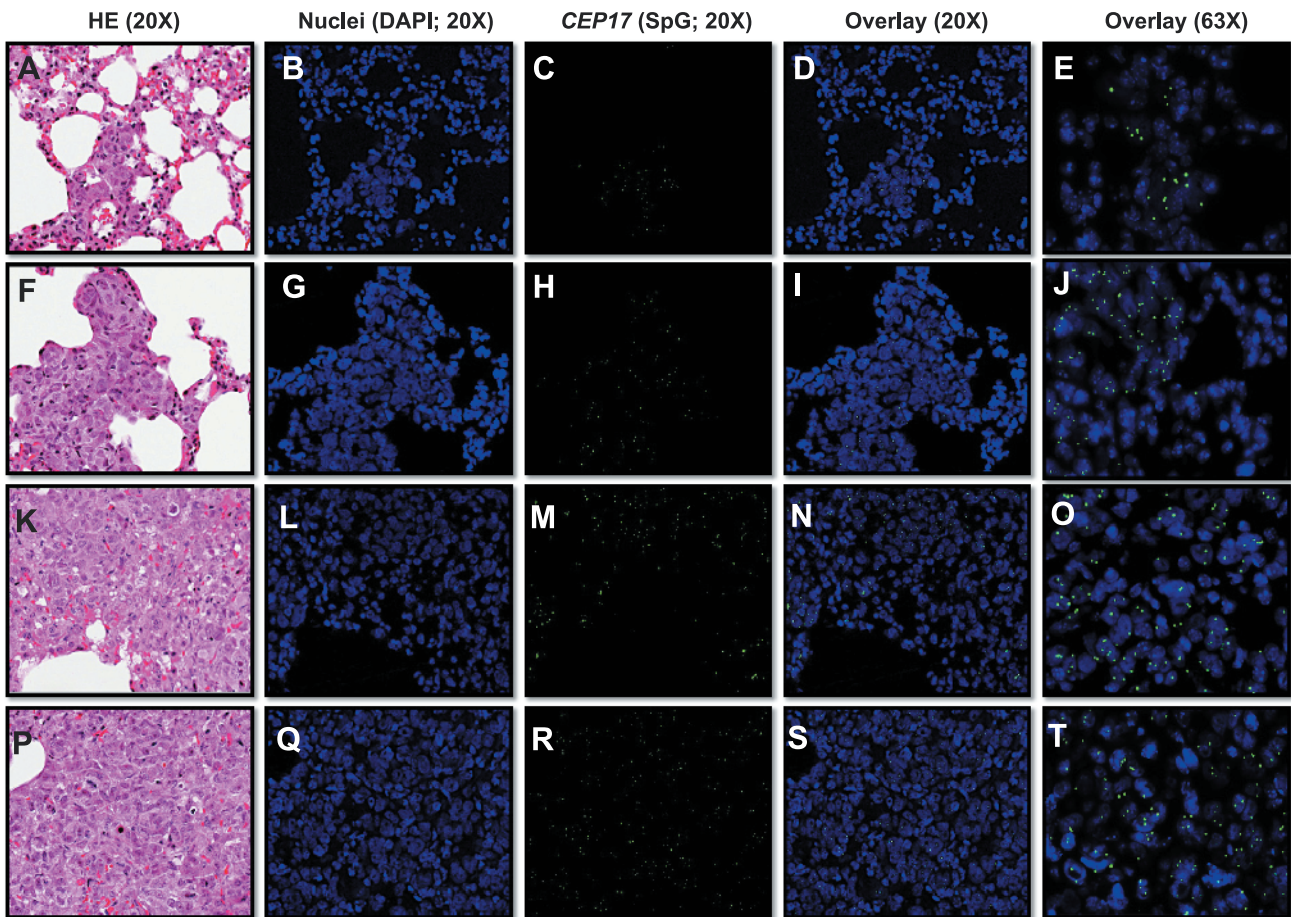
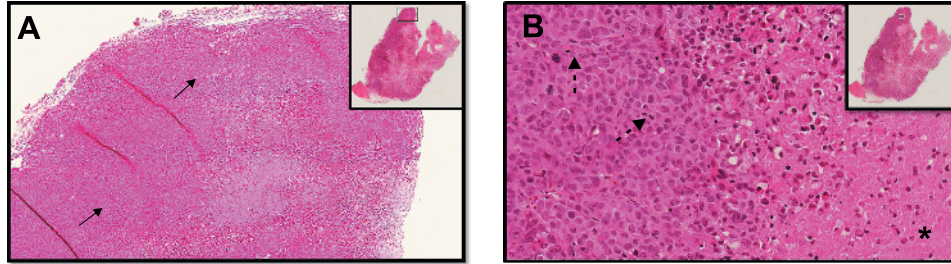


**Figure W1.** Pathologic assessment of pulmonary metastatic tumor load in treatment cohorts. Histology of tumor-bearing mouse lungs after 15 doses of (A) SFN and FPD, (B) SFN, (C) FPD, and (D) vehicle control (PBS), compared with (E) normal lung. Hematoxylin and eosin (HE)-stained lung sections ( $\times 4$ ) showed poorly differentiated carcinoma in both treatment and control groups relative to normal lung. Tumor burden tended to vary between groups, but the pattern of metastasis was diffuse and bilateral in all cases with readily apparent vascular involvement, suggesting a hematogenous route of spread. The morphology of these metastatic lesions resembled that of tumors at the orthotopic engraftment site (see Figure W3), and FISH analysis using a human-specific *Cep17* probe confirmed the neoplastic cells in the lung to be human in origin. (A, B) Isolated nests (arrows) or irregular nodular-like (dashed arrows) distributions of neoplasms with substantial preservation of normal lung histology were evident in the combination and SFN-treated groups (compare with Figure W1E). (C, D) Confluent sheets of neoplastic cells (asterisks) with diffuse involvement of pleura and obliteration of a significant portion of alveolar airspace were apparent in FPD-treated and control cohorts (compare with A and B). (E) Normal BalbC-RAG2<sup>-/-</sup> | IL2R $\gamma$ <sup>-/-</sup> mouse lung showing variably sized alveolar airspaces separated by delicate paucicellular interstitial parenchyma and surrounded by a thin visceral pleura. Corresponding locations of each FFPE section are shown in the right upper inserts.



**Figure W2.** Quantification of pulmonary metastatic tumor load by FISH. Whole lungs were resected from each mouse 35 days post-engraftment and prepared in FFPE tissue blocks ( $n = 24$ ). Five-micrometer sections from each mouse were prepared for species-specific FISH-based detection of metastasized MDA-MB-231 using a *Cep17* SpectrumGreen (SpG) probe and counterstained with DAPI to detect nuclei. Adjacent tissue sections were stained with HE for corresponding pathologic assessment. Representative HE and FISH/DAPI stains of regions in Figure W1, A–D. (A–E) SFN-FPD combination cohort. (F–J) SFN cohort. (K–O) FPD cohort. (P–T) Control cohort. Lungs with the least metastatic burden (A–E) show tumors restricted to the interstitium with preservation of alveolar and vascular architecture, while in the more severely affected lungs (K–O and P–T) tumors have destroyed native parenchymal architecture that completely fill the airspaces. Lungs with a moderate burden of metastasis (F–J) show expansion of the interstitium and destruction of capillaries by tumors, yet alveolar airspaces are maintained.



**Figure W3.** Histology of FFPE primary orthotopic MDA-MB-231 xenograft tumors;  $\times 20$  (A) and  $\times 40$  (B) magnifications of HE-stained FFPE lung sections are shown. Native glandular breast tissue is completely replaced by a high-grade breast carcinoma characterized by a solid growth pattern (arrows), significant nuclear pleomorphism, and numerous mitotic figures (dashed arrows). The tumor extensively infiltrates mammary adipose tissue, and there is abundant central tumor-type necrosis (asterisk). Corresponding location of each FFPE section is shown in the right upper inserts.

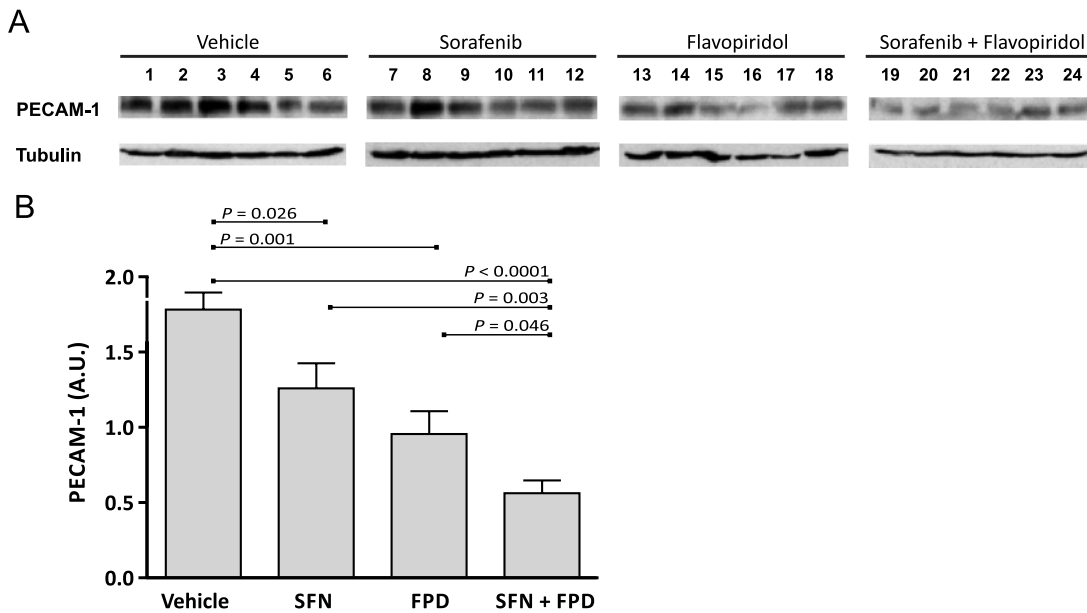


**Figure W4.** Enhanced reduction of CD31 (PECAM-1) expression in tumors isolated from the FPD-SFN-treated cohort. (A) Immunoblots of lysates prepared from resected tumors assessing CD31 expression levels in the indicated cohorts ( $n = 24$ ). Loading was assessed by tubulin levels. (B) Densitometry analyses of the average intensity of CD31 staining. The mean  $\pm$  SEM intensity expressed as a ratio of tubulin intensity across treatment cohorts (six mice/cohort) is shown. Significant  $P$  values ( $t$  test) are indicated. A.U., arbitrary units.